Electron heat transport comparison in the Large Helical Device and TJ-II

J. García[a] and J. Dies
Fusion Energy Engineering Laboratory (FEEL), Departament de Física i Enginyeria Nuclear, ETSEIB, Universitat Politècnica de Catalunya (UPC), Barcelona, Spain

F. Castejón
Laboratorio Nacional de Fusión, Asociación EURATOM-CIEMAT, Centro de Investigaciones Energéticas, Medioambientales y Tecnológicas, Madrid, Spain

K. Yamazaki
Nagoya University, Chikusa-ku, Nagoya 464-8603, Japan

(Received 13 July 2007; accepted 6 August 2007; published online 30 October 2007)

The electron heat transport in the Large Helical Device (LHD) [K. Ida, T. Shimozuma, H. Funaba *et al.*, Phys. Rev. Lett. **91**, 085003 (2003)] and TJ-II [F. Castejón, V. Tribaldos, I. García-Cortés, E. de la Luna, J. Herranz, I. Pastor, T. Estrada, and TJ-II Team, Nucl. Fusion **42**, 271 (2002)] is analyzed by means of the TOTAL [K. Yamazaki and T. Amano, Nucl. Fusion **32**, 4 (1992)] and PRETOR-Stellarator [J. Dies, F. Castejon, J. M. Fontdecaba, J. Fontanet, J. Izquierdo, G. Cortes, and C. Alejaldre, Proceedings of the 29th European Physical Society Conference on Plasma Physics and Controlled Fusion, Montreux, 2002, Europhysics Conference Abstracts, 2004, Vol. 26B, P-5.027] plasma simulation codes and assuming a global transport model mixing GyroBohm-like drift wave model and other drift wave model with shorter wavelength. The stabilization of the GyroBohm-like model by the $E\times B$ shear has been also taken into account. Results show how such kind of electron heat transport can simulate experimental evidence in both devices, leading to the electron internal transport barrier (eITB) formation in the LHD and to the so-called "enhanced heat confinement regimes" in TJ-II when electron density is low enough. Therefore, two sources for the anomalous electron heat transport can coexist in plasmas with eITB; however, for each device the relative importance of anomalous and neoclassical transport can be different. © *2007 American Institute of Physics*. [DOI: 10.1063/1.2779280]

I. INTRODUCTION

Understanding plasma physics is a challenge for the science community, since the processes involved comprise many different physics fields as thermodynamics, electromagnetism, or hydrodynamics. In the resulting framework (and particularly in the controlled magnetic fusion field), the equations involved in the resolution of the main plasma variables are quite difficult to solve analytically due to their highly nonlinear global structure. In this situation, transport codes are a powerful tool to solve the plasma equations obtained from physical theories. Moreover, from the analysis of the results obtained, the experimental data can be better understood, the experiments may be improved, and the performance of future fusion magnetic devices can be predicted in an easier way.

Electron heat transport is a key element in controlled fusion field since high levels of turbulence are present in the actual fusion devices. With the appearance of the electron internal transport barrier (eITB) scenarios, this turbulence can be suppressed in a wide range of the plasma core, as it has been shown in the Large Helical Device (LHD),[1] Compact Helical System (CHS),[2] and TJ-II in the so-called "enhanced heat confinement regimes."[3] These shots have the common feature of having high electron temperature plasmas with peaked profiles as well as high positive electric fields in the plasma core with a large shear. Some theories have been derived to explain the formation of these regimes. The change from the ion root to the electron one seems to be the phenomenon responsible of the eITB formation in LHD and CHS, but it is not clear what role is played by this transition in TJ-II. Thus, no universal explanation for the formation of these regimes has been addressed so far. In particular, the importance of the radial electric field or its shear in the electron heat turbulence suppression is an open issue yet, although the electric field seems to be the key factor.[4]

GyroBohm transport with electron diffusivity dependence on electron temperature scaling as $\chi_e \sim T_e^{1.5}$ has been experimentally found to drive anomalous transport in LHD plasmas with no eITB.[1] Therefore, a GyroBohm-like model has been included in the TOTAL[5] code with the aim of analyzing electron heat transport in the LHD. However, since electromagnetic drift waves may play a role when the eITB is formed and the beta is high,[6] a model that takes into account such transport has been also included. The suppression of the GyroBohm transport by the $E\times B$ shear is also taken into account by calculating the neoclassical radial electric field (E_r), and therefore the $E\times B$ shearing rate.

From previous analysis of the maximum shearing rate [$\max(\omega_{E\times B})$] dependence on average density carried out for the LHD, the eITB formation can be described as a second-order phase transition with critical exponent $\beta=0.4$;[7] how-

[a]Present address: Association Euratom-CEA, CEA/DSM/DRFC, CEA/Cadarache, 13108 St. Paul-les-Durance, France.

ever, in that study, only a GyroBohm model was considered for the electron heat transport. In the framework of this paper, the analysis of $\max(\omega_{E\times B})$ is reconsidered with the inclusion of electromagnetic drift waves in the simulation. Finally, this global framework is applied to the analysis of electron heat transport in the TJ-II device by means of the code PRETOR-Stellarator, which has been previously benchmarked with experimental data from TJ-II,[8] with the aim of doing a comparison of electron thermal transport in both devices.

II. DESCRIPTION OF THE NEOCLASSICAL AND ANOMALOUS TRANSPORT MODELS

The neoclassical model used calculates the axisymmetric tokamak-like part[9,10] and an asymmetric helical part,[11,12] and it has been previously checked for LHD plasmas in Refs. 13 and 14 and for TJ-II plasmas in Ref. 15 by comparing it with MonteCarlo calculations.[16] The expression for the radial asymmetric neoclassical flux associated with helical-ripple trapped particles Γ_j^{na} and heat flux Q_j^{na} of electrons $(j=e)$ and ions $(j=i)$ is given by

$$\Gamma_j^{na} = -\varepsilon_t^2 \varepsilon_h^{1/2} v_{\mathrm{the}j}^2 n_j \int_0^\infty x^{5/2} e^{-x} \tilde{v}_j \frac{A_j(x,E_r)}{\omega_j^2(x,E_r)} dx, \tag{1}$$

$$Q_j^{na} + \frac{5}{2}\Gamma_j^{na} T_j = -\varepsilon_t^2 \varepsilon_h^{1/2} v_{\mathrm{the}j}^2 n_j T_j^2 \int_0^\infty x^{7/2} e^{-x} \tilde{v}_j \frac{A_j(x,E_r)}{\omega_j^2(x,E_r)} dx, \tag{2}$$

where

$$x = m_j v_{\mathrm{the}j}^2 / 2T_j, \tag{3}$$

$$A_j(x,E_r) = n_j'/n_j - Z_j e E_r/T_j + (x-3/2)T_j'/T_j, \tag{4}$$

$$\tilde{v}_j(x) = v_j^0 x^{-1.5} \varepsilon_h^{-1} \left\{ \left[(1-1/2x)\mathrm{erf}(x^{1/2}) + \frac{e^{-x}}{(\pi x)^{1/2}} \right] + \bar{Z}_j \right\} \tag{5}$$

$$\omega_j^2(x,E_r) = 3.0\frac{\tilde{v}_j^2}{F_m/F_s} + 1.5(\varepsilon_t/\varepsilon_h)^{1/2}(\omega_E + \omega_{Bj})^2 + (\varepsilon_t/\varepsilon_h)^{3/2}\left[\frac{\omega_{Bj}}{4} + 0.6|\omega_{Bj}|\tilde{v}_j(\varepsilon_t/\varepsilon_h)^{3/2} \right], \tag{6}$$

$$v_j^0 = \frac{4\pi e^4 n_j \ln\Lambda}{m_j^2 v_{\mathrm{the}j}^3}. \tag{7}$$

Here, the radial flux coordinate is defined as $r=\sqrt{\phi/\pi B_0}$, where ϕ is the toroidal magnetic flux and B_0 is the magnetic field at the axis. The normalized flux coordinate is defined as $\rho=r/a$. ε_t is the toroidal ripple, ε_h is the helical ripple modulation, n_j is the plasma density, T_j is the plasma temperature, $v_{\mathrm{the}j}$ is the thermal velocity, ω_E is the $E\times B$ drift frequency, ω_B is the ∇B drift frequency, and $\bar{Z}_e=Z_{\mathrm{eff}}$ for electrons and $\bar{Z}_i=0$ for ions. The prime denotes the derivative with respect to the radial coordinate.

The factor F_m/F_s takes into account of the multihelicity case in the $1/\nu$ collisional regime by means of the effective ripple previously calculated in the case of the TJ-II device[17] and by means of GIOTA code in the case of LHD.[5] Due to the complicated magnetic structure of TJ-II, it is not enough to consider the first terms of the Fourier series as helical and toroidal ripples, it is necessary to consider the effective values for those quantities. It is quite important in this case because of the TJ-II complicated magnetic field structure. The validity of Eq. (6) for the multihelicity case has been benchmarked in Ref. 5, and the expression for the particle flux shown in Eq. (1) is applicable to both collisionless and collisional regimes for the LHD.[14] In the above equations, the ν regime transport was modified according to Ref. 12 to include the $\nu^{1/2}$ regime.

The geometrical factor ε_h that appears in the neoclassical equations is obtained by means of the equilibrium solver VMEC, with the pertinent corrections in order to take an effective ripple that somehow accounts for the complexity of the TJ-II magnetic configuration. Moreover, the main geometrical factors for both TJ-II and LHD that appear in transport equations (including the geometrical factors $\langle|\nabla r|^2\rangle$ and V') are also estimated from VMEC calculations.

The electron heat transport model can be described as

$$\chi_e = \chi_1 + F(\omega_{E\times B})\chi_2 + \chi_{\mathrm{neo}}, \tag{8}$$

where

$$\chi_1 = C_1 \frac{v_{\mathrm{the}}}{(L_{Te}R)^{1/2}} \frac{c^2}{\omega_{pe}^2}, \tag{9}$$

$$\chi_2 = C_2 (cT_e/eB)(\rho_i/a) \tag{10}$$

and ρ_i is the ion Larmor radius calculated at the electron temperature, $L_{Te}=|\nabla T_e/T_e|^{-1}$, and a the minor radius.

Model from Eq. (9) basically follows the Okhawa scaling[18] and leads to electromagnetic drift wave transport.[19] The expression from Eq. (10) is basically a GyroBohm model with strong dependence on electron temperature $\chi_e \sim T_e^{1.5}$. Since transport by electromagnetic drift waves with small wavelength is not suppressed by the $E\times B$ shear in the formation of eITB in tokamaks,[20] the factor $F(\omega_{E\times B})$ appearing in Eq. (8) is applied only to the GyroBohm transport, which has typical longer wavelength,[6] with the aim of checking whether the same characteristic can also be present in plasmas with eITB in stellarators.

The constants $C1$ and $C2$ have been calculated with the aim of minimizing the differences between the experimental (for shot #26943 in the LHD case and #2562 in the TI-II device) and the estimated electron temperature profiles by least-squares techniques. This minimizing process has been performed for a given time, but $C1$ and $C2$ are kept constant during the full discharge, hence keeping the predictive capability of the simulations. The factor that takes into account of the anomalous transport reduction due to the $E\times B$ flow is the following one:

$$F(\omega_{E\times B}) = [1 + (\tau\omega_{E\times B})^2]^{-1}, \tag{11}$$

where $\omega_{E\times B}$ is calculated by using the following equation:

$$\omega_{ExB} = r\left(\frac{\partial}{\partial r}\right)\frac{E_r}{rB_\theta} \tag{12}$$

with B_θ the poloidal magnetic field.[21] The factors from Eqs. (11) and (12) have been also derived from theoretical models for the anomalous transport suppression in the edge region.[22–24]

The time evolution of E_r is calculated using the following equation:

$$\frac{\partial}{\partial t}E_r = \frac{-e}{\varepsilon_0 \varepsilon_\perp}J_r, \tag{13}$$

where $J_r = \Sigma_k Z_k \Gamma_k^{\text{asym}} - \Gamma_e^{\text{asym}}$ is the radial current, which in helical systems is induced by ripple transport and has a nonlinear dependence on E_r. Γ_e^{asym} is the asymmetric part of the neoclassical electron flux, Γ_k^{asym} and Z_k are the asymmetric neoclassical ion flux and the ion charge for each species k, respectively, $\varepsilon_\perp = (1 + c^2/V_A^2)$, where V_A is the Alfvén velocity and ε_0 is the dielectric constant in vacuum.

The τ values ($\tau = 5.0 \times 10^{-5}$ s in the TJ-II case and $\tau = 5.1 \times 10^{-4}$ s for the LHD) in Eq. (11) were chosen after a sensitivity study. Due to the special feedback between anomalous transport and $F(\omega_{E\times B})$, when τ is higher the temperature tends to increase with no limit, due to the high reduction of the anomalous transport, and when τ is smaller, the effect of $F(\omega_{E\times B})$ is negligible and there is no critical transition between lower and higher confinement regimes. Since the critical $\omega_{E\times B}$ is different for both devices, τ is also different. This means that the plasma is close to the marginality stability, and a similar mechanism has been found in the TJ-II case for the L-H transition.[25] Finally, the value of τ found for the TJ-II, is quite similar to the fluctuation correlation time found for this device.[26]

The transport equations solved in this transport analysis can be found in Ref. 11.

III. ANALYSIS OF THE LHD ELECTRON HEAT TRANSPORT

A. Experimental setup

The LHD is a toroidal helical magnetic device with a major radius of $R_{ax} = 3.5–4.1$ m, an average minor radius of 0.6 m and magnetic field $B_0 = 0.5–3$ T. With the aim of analyzing the model showed in Eq. (8), including the factor that takes into account of the reduction of transport by the $E \times B$ shear, a shot with eITB is firstly analyzed. The shot #26943 corresponds to the fifth campaign of the LHD experiment. The high peaked electron temperature profile has been obtained by using 1 MW of electron cyclotron heating (ECH) power[27] with $B_0 = 2.8$ T and $R_{ax} = 3.5$ m. Figure 1 shows the electron temperature and density profile measured by 200-channel YAG Thomson scattering system[28] and 11-channel Fourier infrared transform interferometer.[29] The density profile was obtained by Abel inversion method with three-dimensional self-consistent equilibrium calculated by using extended radial magnetic coordinates to treat with ergodic regions in the PRE-TOTAL code.

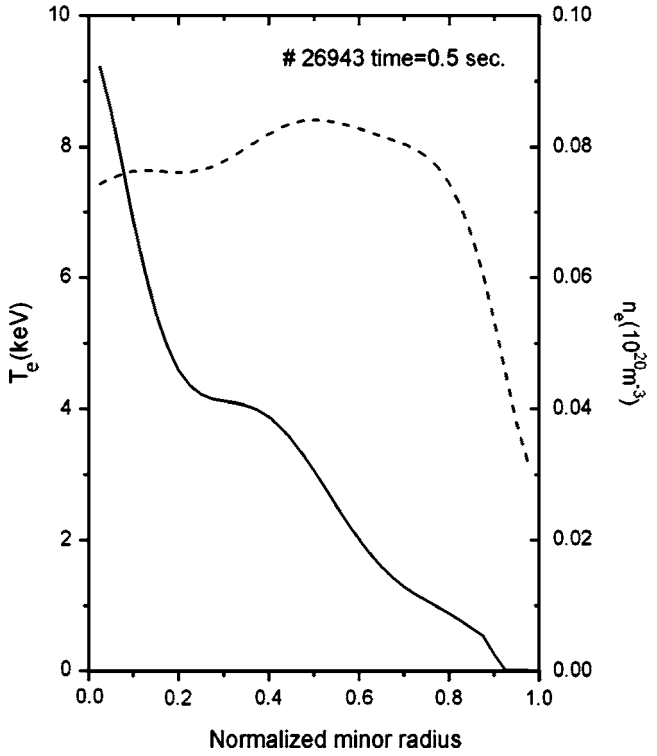

FIG. 1. Experimental profiles of the electron temperature (solid) and density (dashed) obtained in LHD.

Only central value of ion temperature is measured to be 2.0 keV by the crystal spectrometer technique, and the parabolic profile of ion temperature was assumed for equilibrium reconstruction.

The central deposition profile of ECH ray-tracing analysis depends critically on the magnetic axis position and plasma equilibrium, and it is difficult to determine the deposition profile at $\rho < 0.1$. Therefore, we adopted the following profile with the width of $\rho_{wid} = 0.15$:

$$P_{ECH} \propto \frac{1}{\exp[(\rho/\rho_{wid})^4]}, \tag{14}$$

which agrees well with the results of the ray-tracing analysis at $\rho \geqslant 0.1$.

B. Results of the shot #26943 simulation

The model shown in Eq. (8) has been added to the TOTAL code with the aim of simulating shot #26943. In Fig. 2(a), the comparison between the electron temperature profile obtained and the experimental electron temperature is given. An electron temperature profile with a steeped gradient ($dT_e/dr \sim 34$ keV m^{-1}) is obtained, leading to a good agreement with experimental data, mainly in the plasma core. The high temperature gradient is obtained in the region $0 \leqslant \rho \leqslant 0.2$, whereas for $\rho > 0.2$, a flatter profile appears. This a typical behavior expected in an eITB shot in LHD.[1]

Comparing the electron temperature profile with the one obtained in Ref. 11 with just a GyroBohm transport model, we can conclude that the inclusion of an electromagnetic model, which is only important when the $E \times B$ shear is large

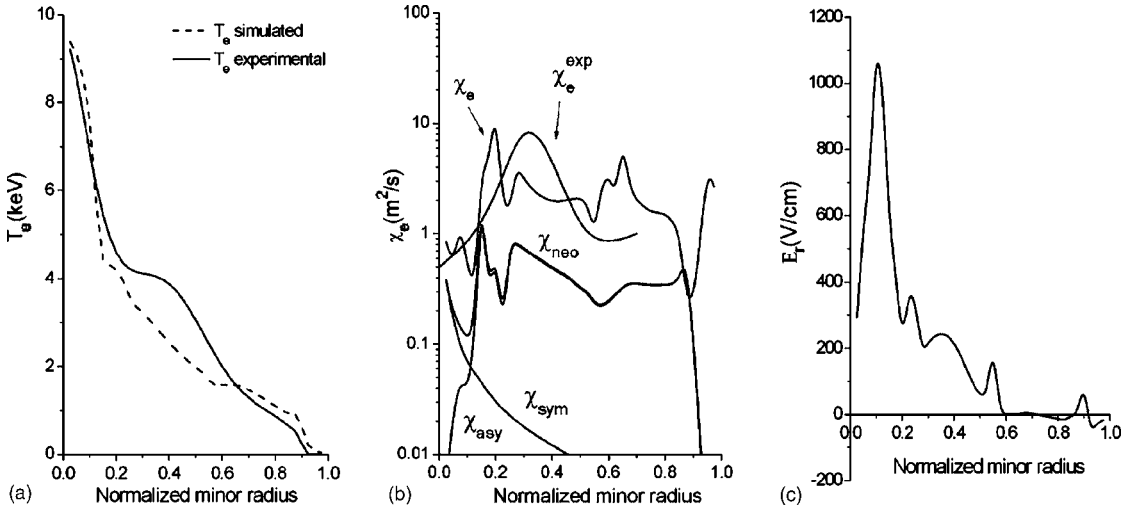

FIG. 2. Comparison between the electron temperature profiles obtained by means of the model from Eq. (8) with the inclusion of the electric field shear effect (solid) and the experimental profile (dashed) (a). Electron thermal diffusivity χ_e obtained with the GyroBohm-like model, asymmetric neoclassical diffusivity χ_{asym}, symmetric neoclassical diffusivity χ_{sym} and total neoclassical diffusivity χ_{neo} (b). Electric field obtained in the simulation (c).

enough to suppress GyroBohm transport, improves the simulation of the electron temperature mainly in the plasma core since no flat profiles are obtained.

It seems clear from Fig. 2(c) that the appearance of the steeped temperature profile is completely linked to the appearance of a high positive electric field ($E_r \approx 1000$ V/cm) with a high shear in the same region $0 < \rho < 0.2$ ($|dE_r/dr| \approx 125$ V/cm^2). Outside this region, the electric field tends to be small with very small electric field shear. This large shear is able to suppress the electron heat transport driven by GyroBohm transport and it leaves electromagnetic transport as the main transport mechanism in the plasma core together with neoclassical transport. Therefore, the eITB formation can be understood as a change of the main transport mechanism in the plasma core due to the appearance of a high sheared $E \times B$ flow. This point will be clarified in the following sections.

1. Analysis of the electron density sensitivity

In Fig. 2(b), electron thermal diffusivities are shown. The electron thermal diffusivity is small in the plasma core and grows up to $\chi_e \approx 10$ m^2/s at $\rho \approx 0.2$. After that, it drops again in the range $0.25 \leqslant \rho < 0.4$. This profile is compatible with the experimental electron heat diffusivity χ_e^{exp}, given also in Fig. 2(b). In addition, this behavior is the one expected from an eITB scenario in the LHD case.[1] Related to neoclassical thermal diffusivities, according to the model applied in this paper, they tend to be always smaller than the total one, even in the plasma core. Comparing these results with the analysis of the fixed temperature and density experimental profiles of shot #26943 performed in Ref. 27, we can conclude that the results fits reasonably well. It is worth to point out that the ion temperature is also simulated in this paper. However, since there is no experimental profile available for the shot #26943 the profile cannot be compared. Anyway, the profile obtained is rather flat, as can be expected from other LHD shots in which the ion temperature profile is available.[1] A sensitivity study about this topic has been done in Ref. 27, showing that only outside the central plasma, the electric field is sensitive to the ion temperature profile. Therefore, the values of the electric field and $\omega_{E\times B}$ obtained in this paper are rather safe in the plasma core, and thus it is the analysis of the eITB formation, which depends mainly on the central values.

The eITB formation in LHD as well as in CHS strongly depends on average density when the input power from ECH is fixed. According to experimental evidence, there is a critical value below which the eITB is formed. In order to check the goodness of the transport model from Eq. (8) to reproduce the eITB formation in the LHD, several simulations have been carried out with the same electron density profile shown in Fig. 1 but with different average densities. As can be seen in Fig. 3(a), there is a clear transition between electron temperature profiles with high steeped gradients, in the case of low average density and rather flat temperature profiles when higher densities are applied. These results are the expected ones in the LHD eITB scenarios[1] as well as in CHS.[2] In order to analyze the transition between both regimes, the central temperature dependence on average density is shown in Fig. 3(b). Clearly, two confinement regimes arise, one with $T_e(0) \propto \langle n_e \rangle^{-0.64}$ and normalized temperature gradient $R/L_{Te} > 25$ for the eITB case, and $T_e(0) \propto \langle n_e \rangle^{-0.44}$ with $R/L_{Te} < 5$ in the non-eITB one, whereas a transition region is in between them. Comparing these results with experimental data,[1] we may conclude that the exponents of the temperature dependence on density are close to experimental LHD evidence (0.60 in the eITB case and 0.43 in the non-eITB one).

Figures 3(a) and 3(b) show how the critical point for the transition between non-eITB and eITB scenarios for this plasma configuration is located in the region $\langle n_e \rangle \approx 0.8 \times 10^{19}$ m^{-3} (reasonably agreeing with experimental data[1]), where a small ITB is formed. In Fig. 3(c) the electric field profile obtained for densities close to the critical region are shown. There is a clear transition from a high electric field with a high shear when the density is below the critical value

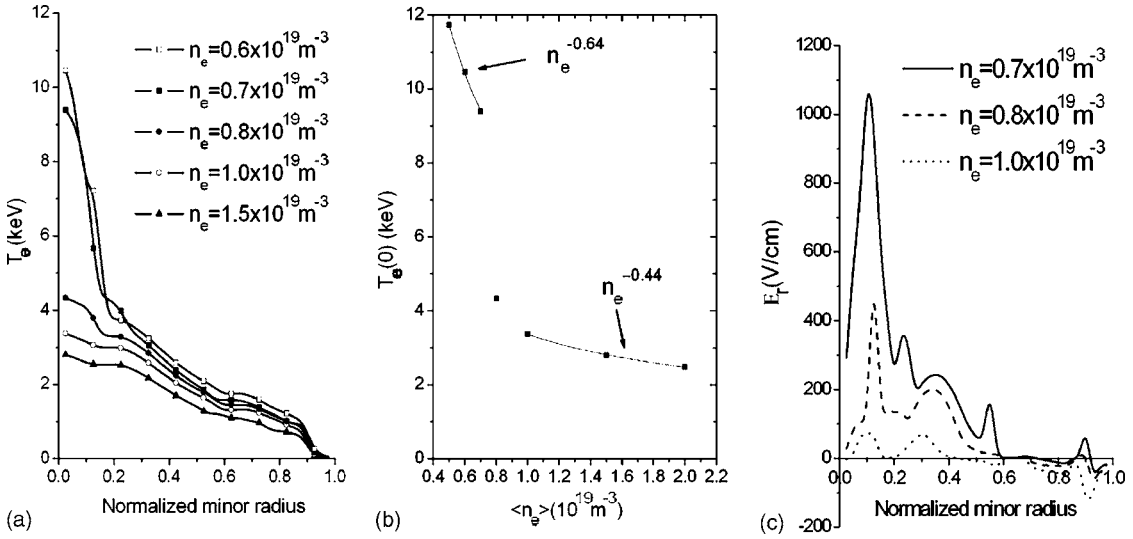

FIG. 3. Electron temperature profiles obtained with the model applied in this paper for each density profile (a). Central electron temperature dependence on average density obtained (b). Comparison between the radial electric field obtained for different average temperatures (c).

and a small electric field with a very low shear when the density is above that value. Therefore, the appearance in the electron root of a high positive sheared electric field is strongly linked with the formation of the eITB.

It is worth pointing out again that the inclusion of the electromagnetic transport, which is only important when the $E\times B$ shear is high enough, i.e., in the plasma core when average density is below the critical point, seems to improve the dependence of central electron temperature on average density, since the previous dependence obtained in Ref. 11 with only a GyroBohm model was $T_e(0)\propto\langle n_e\rangle^{-0.70}$.

This feature seems to confirm the fact that the eITB formation is due to the suppression of GyroBohm transport, but once the eITB is formed, the electron heat transport in the plasma core is not dominated by GyroBohm transport but by electromagnetic drift waves together with some level of neoclassical transport. Therefore, according to the models applied in this paper, transport is dominated by the GyroBohm scaling, i.e., $\chi_e\sim T_e^{1.5}$, below the transition point and by electromagnetic drift waves together with neoclassical transport far above the transition point, whereas both types of turbulences can coexist in the transition region.

In order to get a deeper insight the real time formation of the eITB and its dependence on the total ECH power, a simulation is carried out with $\langle n_e\rangle=1.0\times10^{19}$ m^{-3} [thus, with no eITB according to Fig. 3(a)] but changing from $P_{\mathrm{ECH}}=1$ MW to $P_{\mathrm{ECH}}=1.5$ MW (with the same deposition profile) after 5 s. It is shown in Fig. 4 how a weak eITB is quickly formed after 0.1 s, which means that the ECH power is a critical issue for the eITB formation. However, the behavior of the points $\rho=0.1$ and $\rho=0.15$ is rather different. Whereas in the first case the electron temperature gradient does not almost change, it suddenly increases up to $dT_e/dr\sim20$ keV m^{-1} after 0.15 s at $\rho=0.15$. A similar feature has been obtained previously for $\langle n_e\rangle=0.8\times10^{19}$ m^{-3} and $P_{\mathrm{ECH}}=1$ MW, as has been shown in Fig. 3(a). The reason is that, in the transition region, GyroBohm transport is still important, which means that the temperature has some flat feature. Once the threshold has been crossed and transport is dominated by electromagnetic drift waves, the gradient can grow up again as shown in Fig. 3(a) and highly peaked temperature profiles are again obtained. Similar features have been found recently in experiments.[30]

C. Analysis of the eITB formation as a phase transmission

As it has been shown in the previous section, the electric field transition from the ion root to the electron root has the typical behavior of bifurcation phenomena. Below a critical density the eITB is formed leading to an electron heat transport dominated by electromagnetic drift waves, on the contrary, above that value no eITB is detected. Therefore, the electron density seems to be a clear control parameter of the

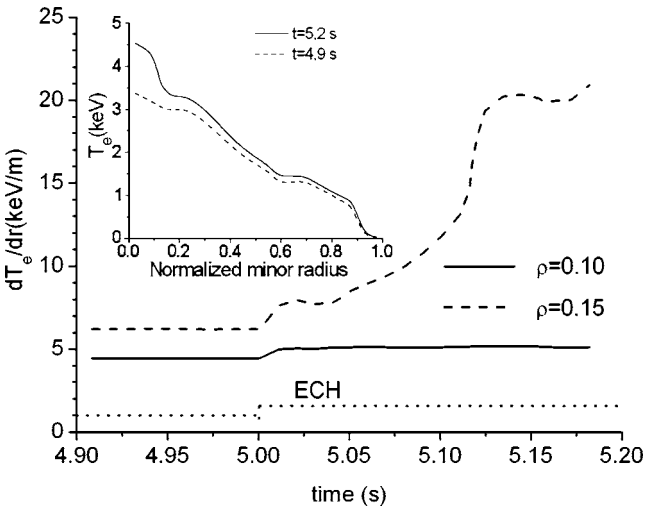

FIG. 4. Electron temperature gradient time evolution for a LHD plasma with $\langle n_e\rangle=1.0\times10^{19}$ m^{-3}. The ECH input power is increased when $t=5$ s from 1.0 to 1.5 MW by keeping its profile. An eITB is formed in a short time, i.e., 50–100 ms, when a small temperature gradient appears at $\rho=0.15$, whereas at $\rho=0.10$ the gradient remains almost unchanged.

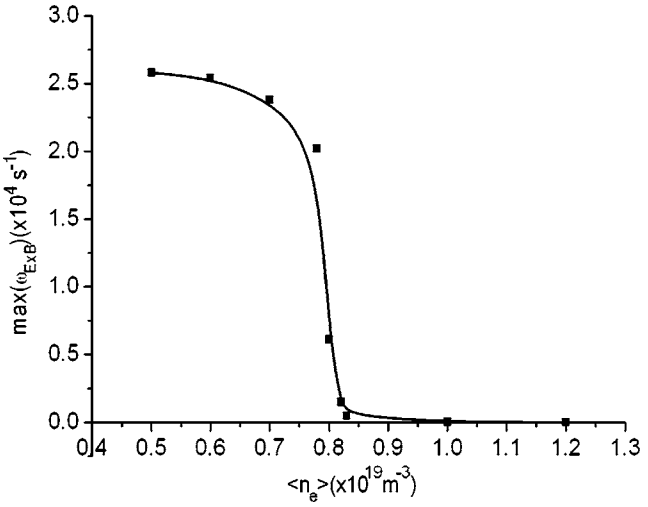

FIG. 5. Order parameter, i.e., $\max(\omega_{E\times B})$, dependence on average electron density. A typical bifurcation point is obtained at $\langle n_e\rangle \approx 0.8\times 10^{19}$ m^{-3}.

eITB formation. In addition, as previously pointed in Ref. 7, the $E\times B$ shearing rate may be understood as a measure of the turbulence levels in the plasma core: low turbulence transport in the eITB scenarios with high searing rate and high transport in non-eITB scenarios with low shearing rate. Therefore, the average density has been chosen as the control parameter and the maximum $E\times B$ shearing rate $[\max(\omega_{E\times B})]$ for each density as the order parameter. Figure 5 shows that a typical bifurcation point is obtained at $\langle n_e\rangle \approx 0.8\times 10^{19}$ m^{-3}. This point divides a region with $\max(\omega_{E\times B})\approx 0$ and another one with $\max(\omega_{E\times B})>0$, corresponding to the eITB formation. The dependence of the order parameter $\max(\omega_{E\times B})$ on the average density can be described as

$$\max(\omega_{E\times B})\begin{cases} \approx 0, & n_e \geqslant n_{ec}, \\ \propto (n_{ec}-n_e)^{\beta}, & n_e < n_{ec}, \end{cases} \tag{15}$$

with $n_{ec}=0.82\times 10^{19}$ m^{-3} and $\beta=0.32\pm 0.09$ is the critical exponent, which is comparable to other critical exponents.[31,32] These values for the β critical exponent have been also obtained using the three-dimensional Ising model.[33]

Since, according to Fig. 5, the order parameter is continuous at the critical point, these results seem to be consistent with a second-order phase transition, which is a feature that has been already stated for the ITB formation in tokamaks.[34] However, due to the extreme nonlinearity of the equations solved, this point must be checked carefully in the future both by means of experimental data and theoretically analysis.[35]

These results seem to confirm two important points: the first one is that the eITB formation in the LHD might belong to the same "universality class" of the ferromagnetic-paramagnetic systems or the liquid-gas mixtures, which have similar critical exponents and therefore, it can be understood as a phase transition, and second, that heat transport by electromagnetic drift waves seem to be important in the plasma core when electron density is low enough.

IV. ANALYSIS OF THE TJ-II DEVICE ELECTRON HEAT TRANSPORT

A. Introduction

Usually, the central electron temperatures obtained in the TJ-II device are about 0.8–1.2 keV with 600 kW electron cyclotron resonance heating (ECRH) nominal injected power. However in low-density scenarios with high ECRH absorbed power density in plasma center, 1.5–2 keV central electron temperature is reached.[3] In these shots, total plasma energy is not substantially increased, since the peaked temperature is localized in a narrow region in plasma centre with small volume, nevertheless, pressure profile shows some improvement of confinement. These scenarios have been called "enhanced heat confinement scenarios," and they are, in some way, different from those with eITB obtained in CHS and LHD, since they are not linked to the transition from the ion root to the electron one. In fact, the electric field obtained in scenarios with and without enhanced heat confinement is positive in the plasma core and it has always one solution of the ambipolar equation. However, the radial electric field as well as the $E\times B$ sheared flow may still play an important role in the enhanced heat scenarios since in these shots the maximum electric field is increased in the plasma core by a factor between 2 and 3.[36] In this situation, a common process could explain the reduction of heat transport in plasma center in LHD and TJ-II. For this purpose, a complete study of electric field is necessary in order to understand the formation of these regimes.

With the aim of analyzing whether the same transport mechanism can explain both the electron heat transport in LHD (including the eITB formation) and the enhanced heat confinement scenarios in TJ-II, the transport model given in Eq. (8) has been added to the PRETOR-Stellarator transport code, and a simulation of the electron temperature profile has been carried out.

B. Experimental setup

The data for the analysis are collected from the TJ-II device, which is a medium size four-period stellarator (heliac type, $B_0\leqslant 1.2$ T; $R_{ax}=1.5$ m; $a\leqslant 0.2$ m) with a wide rotational range $0.9<\iota/2\pi<2.2$ in low, negative shear configurations ($\Delta q/q<-6\%$). The TJ-II plasmas are produced and heated with electron cyclotron resonance heating, performed by two gyrotrons of 300 kW, each at 53.2 GHz, second-harmonic and X-mode polarization.

The shots analyzed are the #2559 and the #2562, which correspond to a density scan.[3] The magnetic configuration used is the 100_40_63 (the figure stands for the currents that circulate by TJ-II coils) that is characterized by having vacuum rotational transform at the center of $\iota(\rho=0)/2\pi=1.51$ and at the edge $\iota(\rho=1)/2\pi=1.61$, above the 3/2 rational value. The plasma composed by hydrogen is heated with 300 kW of ECR heating provided by one gyrotron and transmitted to the plasma by a quasi-optic transmission line. The power deposition is on-axis and its profile is obtained by heat wave propagation experiments.[37]

The electron temperature and density profiles, measured

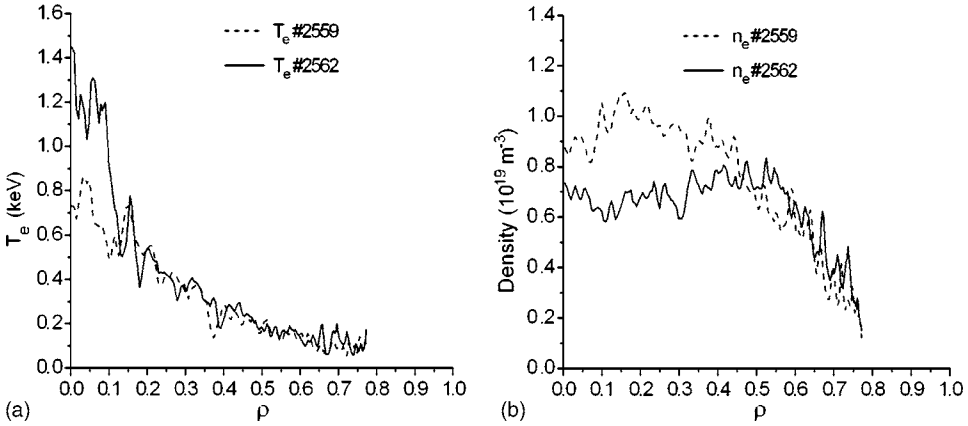

FIG. 6. Electron temperature (a) and density (b) profiles collected from Thomson scattering in shots #2559 and #2562.

by multipoint Thomson scattering profiles,[38] are shown in Fig. 6. It is clear from Fig. 6(a) that, in the low density case, a high temperature gradient appears in the plasma core at $\rho \approx 0.1$, both profiles being quite similar outside that zone. These profiles with stepped gradients have been called enhanced heat scenarios, and they are in some way similar to those obtained in LHD when the density is low enough, however as it is going to be shown further, this feature is not related to the transition form the ion root to the electron one.

C. Results of the shot #2559 and #2562 simulation

A simulation is carried out with the models previously described. The results of temperature simulation compared with experimental data are shown in Fig. 7(a) for shot #2562 and in Fig. 7(b) for shot #2559, whereas the neoclassical electric field structure obtained for both shots is shown in Fig. 7(c).

As can be seen from the graphics, experimental temperatures are simulated with reasonable accuracy by this transport model, leading to a steeped electron temperature profile in the plasma core for shot #2562 and quite flat in the case of shot #2559. The neoclassical electric field has a high positive value, i.e., $E_r \approx 115$ V/cm, in the plasma core for the #2562 shot and a small one, i.e., $E_r \approx 40$ V/cm, for the standard shot #2559. Edges values have positive or negative values alternatively. The measured radial electric field in plasmas which present enhanced heat confinement is in the range of 100–150 V/cm, and without this feature is in the range 40–50 V/cm;[37] hence, the results obtained in this paper with the neoclassical model shown in Eq. (1)–(7) seem to give rise to good agreement with experimental data. In addition to the increasing of the electric field, its shear also grows up from $dE_r/dr \approx 120$ kV m^{-2} up to $dE_r/dr \approx 310$ kV m^{-2}, and this fact leads to an increasing of the $E \times B$ sheared flow, which can be important, according to the transport model applied in this paper, in the reduction of anomalous transport. However, it is worth pointing out at his stage the clear difference between the eITB formation in the LHD previously studied and the formation of this enhanced heat confinement. In the case of TJ-II, the formation is not related to the transition from the ion root to the electron root as shown in Fig. 7(c). The relative importance of the $E \times B$ shared flow in the formation of these scenarios will be discussed in the next section.

The total electron thermal diffusivity as well as the neoclassical one obtained for each shot are shown in Fig. 8. The electron heat diffusivity in the plasma core for the shot #2562 is smaller than in the #2559 case. However, in the

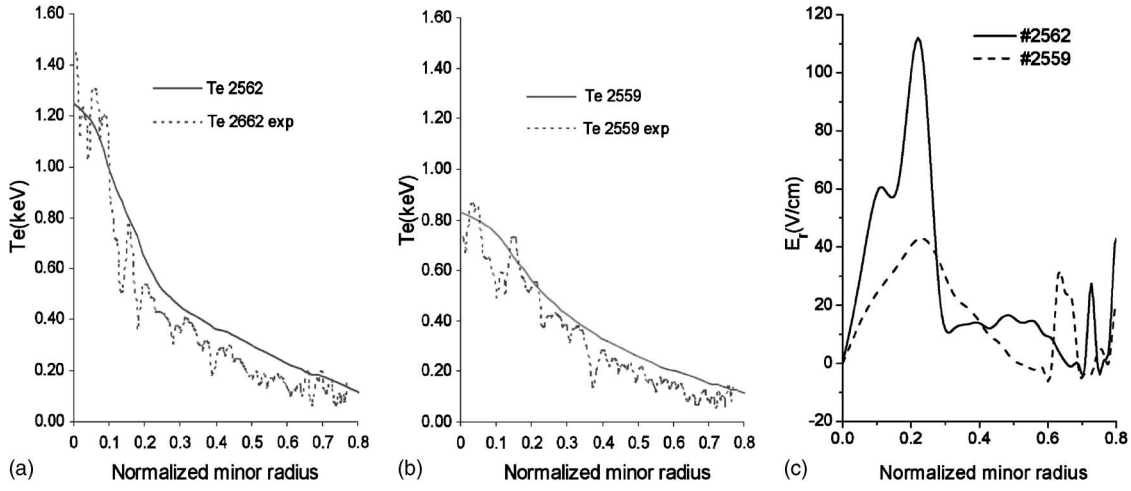

FIG. 7. Comparison between simulated (solid) and experimental electron temperature profile (dashed) of shots #2562 (a) and #2559 (b). Neoclassical electric field obtained by means of the simulation in the case of the shot #2562 (solid) and #2559 (dashed).

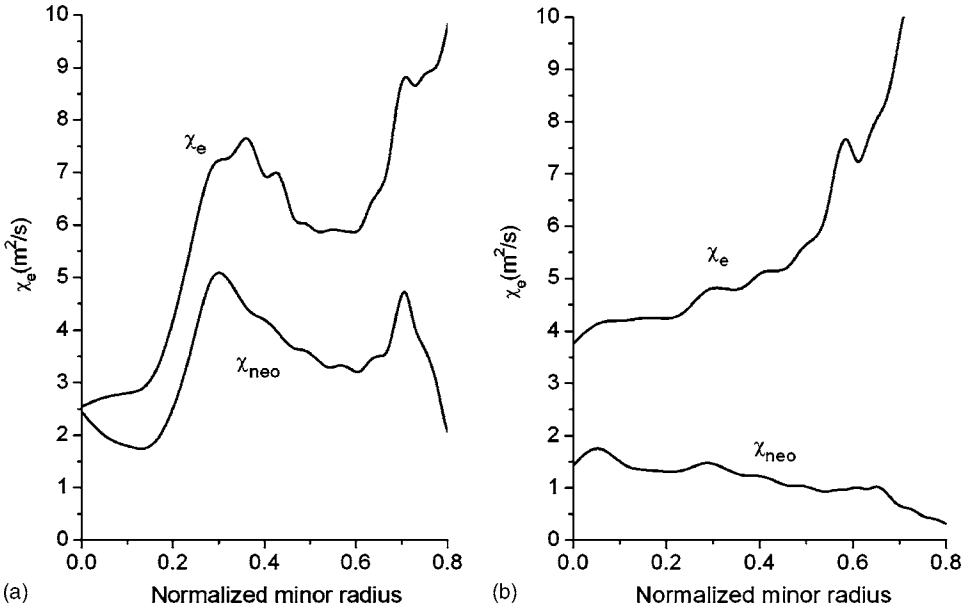

FIG. 8. Electron thermal diffusivity χ_e obtained with the model applied in this paper, and neoclassical diffusivity χ_{neo} in the case of the shot #2562 (a) and #2559 (b).

case of shot #2562 and for $0.2<\rho<0.6$, χ_e increases up to $\chi_e \approx 7\ \mathrm{m^2\ s^{-1}}$, whereas in the #2559 case $\chi_e \approx 4\ \mathrm{m^2\ s^{-1}}$ and it is quite flat for that range. Finally, for $\rho>0.6$, χ_e tends to increase in both cases. Very similar electron heat diffusivity shapes have been obtained from the direct analysis of both shots performed in Ref. 3, although smaller heat diffusivities were obtained in the plasma core in that study. It seems clear from Fig. 7(a) that the increasing of χ_e in the case of shot #2562 for $0.2<\rho<0.6$ is due to the neoclassical transport (the asymmetric part), which is larger than in the #2559 case.

The relative importance of neoclassical transport over the total one is not really enhanced in shot #2562 except in the very inner plasma core, where, according to this model, transport is almost neoclassical for that shot. Outside the zone $\rho<0.1$, neoclassical transport represents approximately around 40% of the total transport in the case of shot #2559 and 60% for shot #2562 in the range $0.1<\rho<0.6$, being almost negligible in the edge.

D. Analysis of the density dependence

It has been shown in the previous section that electron density is a key factor for the formation of the enhanced heat scenarios in TJ-II as it was for the formation of the eITB in LHD. In order to check whether these scenarios with enhanced transport in TJ-II share the same density dependence on average density like the one obtained for the LHD in Sec. III B, a density study performed with the model from Eq. (8) is carried out. In order to perform this study, an electron density profile with a flat zone up to $\rho=0.6$ and decreasing towards the edge has been chosen as a typical density profile for the TJ-II. Several average densities have been applied in order to get the order parameter $\max(\omega_{E\times B})$. Results of the simulation can be found in Fig. 9.

The order parameter shape is similar to the one obtained in the LHD case and a typical bifurcation point is obtained at $\langle n_e\rangle \approx 8.0\times 10^{18}\ \mathrm{m^{-3}}$ that divides two zones, one with $\max(\omega_{E\times B})\approx 0$ and another with $\max(\omega_{E\times B}) \gg 0$. The critical point obtained in this paper in pretty close to the experimental one obtained for TJ-II shots with on-axis ECRH obtained by means of impurity poloidal rotation measurements.[39] Applying Eq. (15) to the data obtained, we get the following values: $n_{ec}=8.1\times 10^{18}\ \mathrm{m^{-3}}$ and $\beta=0.48\pm 0.03$. In this case, the β obtained is higher than in the LHD study, but it still belongs to the range $0.3<\beta<0.5$ like other physical systems showing critical phenomena, and in particular this value is quite close to the one obtained for critical systems obtained with the mean field theory.[35]

From Fig. 9, the role played by the $E\times B$ flow in the enhanced heat confinement shots appeared in TJ-II is clarified. The region where GyroBohm anomalous transport can

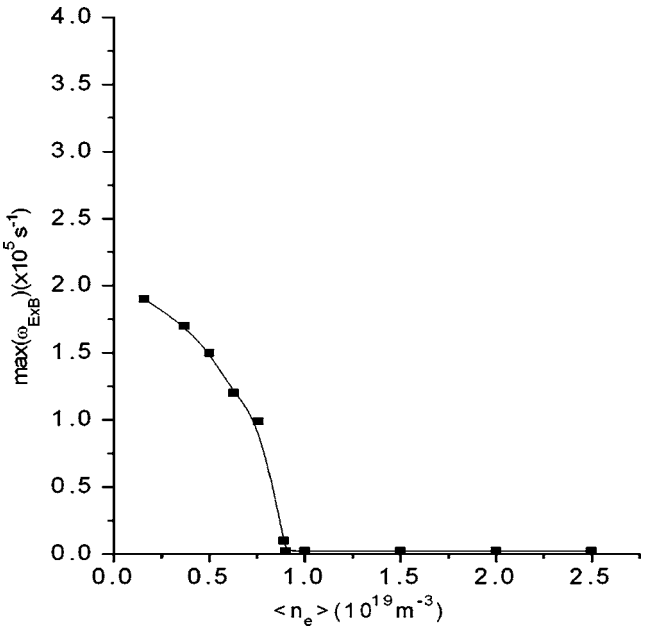

FIG. 9. Order parameter, i.e., $\max(\omega_{E\times B})$, dependence on average electron density for the TJ-II. A typical bifurcation point is obtained at $\langle n_e\rangle \approx 8.0\times 10^{18}\ \mathrm{m^{-3}}$.

be more effectively reduced is close to the transition point from the ion root to the electron one, where for small variations of the average density, really different values of the $E\times B$ flow are obtained. However, the density scan performed in shots #2562 and #2559 (4.5×10^{18} m$^{-3}<n_e<5.5\times10^{18}$ m^{-3}) is far from this transition point and therefore, according to Fig. 9, small variations in the average density do not lead to really high differences in the $E\times B$ flow compared to those obtained close to the bifurcation point. Therefore, although the electric field shear still plays a role in the formation of the enhanced heat confinement shots, most of the anomalous transport suppression by this mechanism has already occurred for higher densities.

The situation is completely different in the formation of the eITB scenarios in LHD since according to Fig. 5, this formation is completely linked to the appearance of a critical point in the $E\times B$ flow and therefore the importance of the electric field shear is really high. Once the eITB is formed and the average density is far form the transition point, the relative importance of the $E\times B$ sheared flow decreases, like in the TJ-II case.

Finally, and according to the models applied in this paper, the importance of neoclassical electron heat transport in both devices seems to be quite different. Whereas in the case of LHD, as shown in Fig. 2(b), neoclassical transport does not play an important role even in the case of eITB scenarios, in the TJ-II case it contributes highly to the total transport in both high and low density regimes. Moreover, in the case of shot #2562, the electron heat diffusivity is strongly determined by neoclassical transport in the plasma range $\rho<0.6$. Thus, the importance of the radial electric field in the formation and modulation of the enhanced heat confinement regimes in TJ-II can be more important than the $E\times B$ sheared flow when the density is far from the transition point from the ion root to the electron one.

V. CONCLUSIONS

The electron heat transport has been studied in LHD and TJ-II devices by means of a transport model that takes into account of GyroBohm transport together with a drift wave model with shorter wavelength. The suppression of turbulent transport by the $E\times B$ sheared flow has been taken into account as a possible mechanism for the eITB formation.

It has been shown that this transport model is able to simulate the shot #26943 from the LHD, as well as, the dependence of central electron temperature on the average density for both high and low density regimes. It seems clear that, according to the models applied in this paper, the transition from a small electric field with no shear to a high positive one with high shear is responsible of the formation of the eITB. At the critical density transition, both types of transport can coexist, however when the density is below that point, electromagnetic drift waves seem to be dominant, whereas GyroBohm transport is more important for higher densities. Therefore, eITB formation in LHD can be regarded as a phase transition between different plasma regimes.

This critical plasma behavior, which leads to the LHD eITB formation, has been characterized as a phase transition by assuming the average density as the control parameter and the maximum $E\times B$ shearing rate as the order parameter. From the analysis, it is deduced that the eITB formation can be described as a phase transition with critical exponent $\beta=0.32\pm0.09$. This critical exponent is comparable to other critical exponents of different phase transition; e.g., ferromagnetic and liquid phase transitions. According to the calculations made in this paper, the critical parameter is continuous at the transition point, which means that the phase transition might be a second-order phase transition, as it has been point in the case of tokamaks. However, much more studies must be done in order to confirm this result.

The electron heat transport has been also studied in TJ-II by analyzing two experimental shots, #2562 (with enhanced heat confinement) and #2559, corresponding to a density scan. The results of the global simulations show that the anomalous transport model used reproduces reasonably well the temperature profile, the radial electric field and the experimental heat diffusivity of both shots. This fact leads to the conclusion that, as in the LHD case, a transport model with GyroBohm transport, electromagnetic drift waves as well as with $E\times B$ shearing rate anomalous transport suppression, is able to simulate heat transport in TJ-II. However, some differences between the eITB formation in LHD and the enhanced heat confinement regimes in TJ-II arise from the analysis. In the case of TJ-II, the electric field obtained for the average density range considered in this study is always positive, and therefore, the formation of these regimes cannot be linked to the transition from the ion root to the electron one.

In order to make a deeper insight in this fact, a study of the dependence of the maximum $E\times B$ shearing rate on average density has been carried out. It has been shown that, as well as in the LHD case, it shows the typical critical behavior of a second-order phase transition with bifurcation point at $\langle n_e\rangle\approx8.0\times10^{18}$ m^{-3} (which is very close to experimental evidence[34]) and with critical exponent $\beta=0.48\pm0.03$. Therefore, although the $E\times B$ suppression still plays a role for these regimes, it seems clear from Fig. 9 that small variations of the density do not lead to really high differences on the $E\times B$ sheared flow because the densities considered are far from the transition point and most of the turbulence driven by GyroBohm transport has been already suppressed.

In addition, and according to the models applied, neoclassical transport is much important in TJ-II than in LHD. In fact, the heat diffusivity for shot #2562 is highly determined by neoclassical transport. Related to anomalous transport, high levels of electromagnetic drift waves can be expected in the plasma core for the shots considered, since GyroBohm transport has been highly reduced. Thus, the relative importance of the radial electric field in the formation of these enhanced heat confinement shots seems to be higher than the $E\times B$ sheared flow, since this electric field highly determines neoclassical transport. Therefore, the so-called scenarios with eITB in stellarators should be deeply analyzed, since although they may share a global transport mechanism, as it has been shown in this paper, the relative

importance of the electric field, its shear, electromagnetic drift waves, GyroBohm transport or neoclassical transport can be quite different.

ACKNOWLEDGMENTS

This work has been supported by Spanish Ministry of Education and Science project ENE2004-05647-FTN.

[1] K. Ida, T. Shimozuma, H. Funaba *et al.*, Phys. Rev. Lett. **91**, 085003 (2003).
[2] A. Fujisawa, H. Iguchi, T. Minami *et al.*, Phys. Rev. Lett. **82**, 2669 (1999).
[3] F. Castejón, V. Tribaldos, I. García-Cortés, E. de la Luna, J. Herranz, I. Pastor, T. Estrada, and TJ-II Team, Nucl. Fusion **42**, 271 (2002).
[4] F. Castejón, A. Fujisawa, K. Ida, J. N. Talmadge, T. Estrada, D. López-Bruna, C. Hidalgo, L. Krupnik, and A. Melnikov, Plasma Phys. Controlled Fusion **47**, B53 (2005).
[5] K. Yamazaki and T. Amano, Nucl. Fusion **32**, 4 (1992).
[6] J. Garcia, K. Yamazaki, J. Dies, and J. Izquierdo, Plasma Phys. Controlled Fusion **48**, 15 (2006).
[7] J. Garcia, K. Yamazaki, J. Dies, and J. Izquierdo, Phys. Rev. Lett. **96**, 105007 (2006).
[8] J. Dies, F. Castejon, J. M. Fontdecaba, J. Fontanet, J. Izquierdo, G. Cortes, and C. Alejaldre, Proceedings of the 29th European Physical Society Conference on Plasma Physics and Controlled Fusion, Montreux, 2002 [Europhys. Conf. Abstr. **26B**, 5.027 (2004)].
[9] F. L. Hinton and R. D. Hazeltine, Rev. Mod. Phys. **48**, 239 (1976).
[10] K. C. Shaing and J. D. Callen, Phys. Fluids **26**, 3315 (1983).
[11] C. S. Chang and F. L. Hinton, Phys. Fluids **25**, 1493 (1982).
[12] E. C. Crume, K. C. Shaing, S. P. Hirshman, and W. I. Van Rij, Phys. Fluids **31**, 11 (1988).
[13] K. Yamazaki, S. Kubo, K. Narihara, K. Tanaka, T. Minami, CHS Group, and LHD Experimental Group, Proceedings of the 29th European Physical Society Conference on Plasma Physics and Controlled Fusion, Montreux, 2002 [Europhys. Conf. Abstr. **26B**, 1.078 (2004)].
[14] S. Toda and K. Itoh, Plasma Phys. Controlled Fusion **44**, 325 (2002).
[15] J. Garcia, K. Yamazaki, J. Dies, F. Castejón, H. Funaba, T. Amano, J. M. Fontdecaba, J. Fontanet, F. Albajar, and J. Izquierdo, J. Plasma Fusion Res. **6**, 481 (2004).
[16] V. Tribaldos, Phys. Plasmas **8**, 1229 (2001).
[17] B. Seiwald, V. V. Nemov, S. V. Kasilov, and W. Kernbichler, Proceedings of the 29th European Physical Society Conference on Plasma Physics and Controlled Fusion, Montreux, 2002 [Europhysics Conference Abstracts **26B**, 4.099 (2002)].
[18] T. Ohkawa, Phys. Lett. **67A**, 35 (1978).
[19] H. Horton, B. Hu, J. Q. Dong, and P. Zhu, New J. Phys. **5**, 14.1 (2003).
[20] B. Esposito, F. Crisanti, V. Parail *et al.*, Plasma Phys. Controlled Fusion **45**, 933 (2003).
[21] K. Itoh, S. Toda, A. Fujisawa, S.-I. Itoh, M. Yagi, A. Fukuyama, P. H. Diamond, and K. Ida, Phys. Plasmas **14**, 020702 (2007).
[22] K. C. Shaing, G. S. Lee, W. A. Houlberg, and E. C. Crume, Jr., in *Plasma Physics and Controlled Nuclear Fusion Research* (International Atomic Energy Agency, Vienna, 1989), Vol. II, p. 13.
[23] K. C. Shaing, E. C. Crume, Jr., and W. A. Houlberg, Phys. Fluids B **2**, 1496 (1990).
[24] C. F. Figarella, S. Benkadda, P. Beyer, X. Garbet, and I. Voitsekhovitch, Phys. Rev. Lett. **90**, 015002 (2003).
[25] C. Hidalgo, M. A. Pedrosa, E. Sánchez *et al.*, Plasma Phys. Controlled Fusion **48**, S169 (2006).
[26] C. Hidalgo, M. A. Pedrosa, and B. Gonçalves, New J. Phys. **4**, 51.1 (2002).
[27] K. Yamazaki, K. Minami, K. Narihara, K. Tanaka, and S. Kubo, J. Plasma Fusion Res. **5**, 611 (2002).
[28] K. Narihara, I. Yamada, H. Hayashi, and K. Yamauchi., Rev. Sci. Instrum. **72**, 1122 (2001).
[29] K. Kawahata, K. Tanaka, Y. Ito, A. Ejiri, and S. Okajima, Rev. Sci. Instrum. **70**, 707 (1999).
[30] K. Ida, Y. Sakamoto, S. Inagaki *et al.*, Proceedings of the 21st IAEA Fusion Energy Conference (IAEA-2006), Chengdu, 2006, IAEA-CN-149/EX/P4-39.
[31] K. Stierstadt, Phys. Bl. **39**, 377 (1990).
[32] J. S. Rowlinson and F. L. Swinton, *Liquids and Liquid Mixtures*, 3rd ed. (Butterworths, London, 1982).
[33] J. C. Le Guillou and J. Zinn-Justin, Phys. Rev. B **21**, 3976 (1980).
[34] P. Mantica, D. Van Eester, X. Garbet *et al.*, Phys. Rev. Lett. **96**, 095002 (2006).
[35] E. M. Lifshitz and L. P. Pitaevskii, *Statistical Physics* (Pergamon, New York, 1980).
[36] F. Castejón, M. Ochando, T. Estrada *et al.*, Proceedings of the 31st European Physical Society Conference on Plasma Physics and Controlled Fusion, London, 2004 [Europhys. Conf. Abstr. **28B**, 4.177 (2004)].
[37] S. Eguilior, F. Castejón, E. de la Luna, A. Cappa, K. Likin, A. Fernández, and TJ-II Team, Plasma Phys. Controlled Fusion **45**, 105 (2003).
[38] J. Herranz, I. Pastor, F. Castejón, E. de la Luna, I. García-Cortés, C. J. Barth, E. Ascasíbar, J. Sánchez, and V. Tribaldos, Phys. Rev. Lett. **85**, 4715 (2000).
[39] B. Zurro, A. Baciero, D. Rapisarda, V. Tribaldos, and TJ-II Team, Fusion Sci. Technol. **50**, 403 (2006).